Spectral Curve Fitting for Automatic Hyperspectral Data Analysis

Adrian Jon Brown

***Abstract*—Automatic discovery and curve fitting of absorption bands in hyperspectral data can enable the analyst to identify materials present in a scene by comparison with library spectra. This procedure is common in laboratory spectra, but is challenging for sparse hyperspectral data. A procedure for robust discovery of overlapping bands in hyperspectral data is described in this paper. The method is capable of automatically discovering and fitting symmetric absorption bands, can separate overlapping absorption bands in a stable manner, and has relatively low sensitivity to noise. A comparison with techniques already available in the literature is presented using simulated spectra. An application is demonstrated utilizing the shortwave infrared (2.0–2.5 μm or 5000–4000 cm^{-1}) region. A small hyperspectral scene is processed to demonstrate the ability of the method to detect small shifts in absorption wavelength caused by varying white mica chemistry in a natural setting.**

***Index Terms*—Curve-fitting, hyperspectral.**

I. Introduction

HYPERSPECTRAL data analysis is often viewed as a statistical pattern recognition problem in a three-dimensional (3-D) hyperspace, often envisaged as a hyperspectral data cube. These analysis methods usually adopt a statistical approach to find image "end members." Statistical methods range from simple hierarchical cluster analysis to complex methods such as minimum noise transforms and the "hourglass" method [1]–[3].

In contrast to these statistical methods, a more traditional spectroscopic approach can be taken, where the analyst concentrates on recognizing absorption band shapes in each individual spectrum. This has the advantage of a direct connection between the reflectance spectrum of the target pixel and its chemical composition. When the hyperspectral dataset is viewed in this way, classifications are made according to underlying physical properties, rather than simply on their similarity to other pixels in the dataset.

Hyperspectral curve fitting methods immediately confront the challenge of modeling multiple overlapping absorption bands with relatively low spectral resolution. Typically, a hyperspectral spectrum has 100–250 measurement points (channels), with a spectral resolution per channel of 10–20 ηm and similar sampling intervals [4], [5]. Typical laboratory spectroscopic instruments have a spectral resolution of 1.25 ηm (2 cm^{-1}) and similar sampling intervals [6]. The order of magnitude difference in spectral resolution means that hyperspectral spectra are not as definitive as laboratory spectra, and curve fitting techniques from the laboratory cannot simply be transferred to hyperspectral studies.

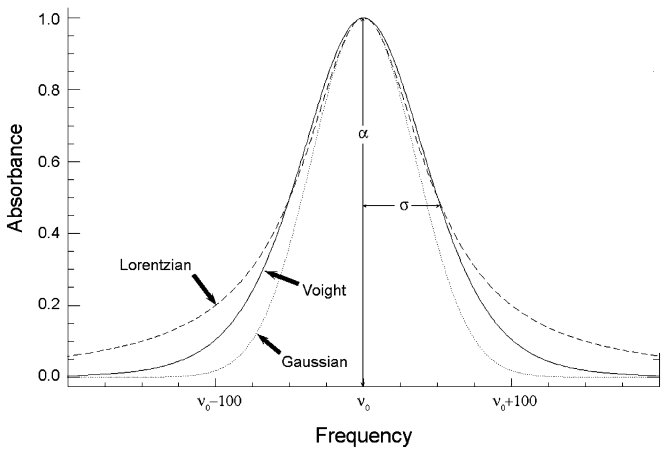

Fig. 1. Comparison of Gaussian, Lorentzian, and Voight functions describing an ideal, symmetrical absorption band. For each function, $\alpha = 1, \sigma = 100$. The Voight function has been generated as described in the text, with $\beta = 0.5$.

Reflectance spectra of solid surfaces can be modeled as a series of deep dips due to absorption bands, superimposed on a background continuum [7]. The central frequency at which absorption bands are detected is of most interest to spectroscopists, since these frequencies are indicative of the mineral types present [8].

Major spectral contributors to a pixel can be discerned by identification of absorption bands. Mixing of spectrally active components, while important, does not obscure all unique characteristics of the major contributors, particularly in the shortwave infrared (SWIR) (2.0–2.5 μm) region, where there exist clearly discernable hydroxyl (OH^-) related absorption bands that are characteristic of geologically important minerals [9].

Derivative spectroscopy can be used to approximate the locations of absorption bands using second and higher degree differential spectra [10], [11]. Fifth-order derivatives have been demonstrated to give the most accurate results [12].

Curve fitting of spectra can estimate not only the central wavelength of the absorption band, but also their width and amplitude of the absorption band (Fig. 1). This is typically achieved using an iterative least squares method [13].

The absorption band dips can be modeled using Gaussian [14], [15], Lorentz [16], or mixed Gaussian–Lorentz (Voight) curves [17]. These curves are all symmetrical shapes that decay

Manuscript received April 4, 2005; revised November 22, 2005.

This paper has supplementary material that is available for download at http://ieeexplore.ieee.org, provided by the authors. This includes a PDF file containing the color version of Fig. 2.

The author is with the Australian Centre for Astrobiology, Macquarie University, Sydney 2109, Australia (e-mail: abrown@els.mq.edu.au).

Digital Object Identifier 10.1109/TGRS.2006.870435

from a central peak (Fig. 1). Differing decay rates make each curve type better at replicating different physical processes [18].

Overlapping absorption bands are additive when measured in an absorption experiment. Reflectance spectra can be converted to apparent absorbance by taking the logarithm of the reflectance

$$\text{apparent absorbance} = \log_{10}(\text{reflectance}). \tag{1}$$

Natural logarithm (sometimes called the Naperian form) is used in the physics community. This procedure uses base 10 logarithm (sometimes called decadic form) since it is the standard in the chemistry and planetary sciences community [14], [15], [19].

Hyperspectral analysts typically report spectra in units of μm or ηm (wavelength), however plotting in energy space in cm^{-1} (wavenumbers) has greater physical basis and eliminates asymmetry due to display on a constant interval wavelength abscissa [20]

$$\text{frequency}(\text{cm}^{-1}) = \frac{10\,000}{\text{wavelength}(\mu\text{m}).} \tag{2}$$

In the remainder of this paper, the mathematics surrounding this curve fitting algorithm will be briefly discussed, followed by analysis of a noise-free and noisy-synthetic spectrum. Fits using Gaussian, Lorentzian, and Voight curves will be compared. Finally, a real-world application will be presented.

II. Methodology

If we consider a continuum removed reflectance spectrum [21], recorded at N discrete points, as a one-dimensional vector $\boldsymbol{R}$, in wavelength space

$$\boldsymbol{R}(\lambda) = R(\lambda_1), R(\lambda_2) \ldots R(\lambda_N). \tag{3}$$

We may convert to apparent absorbance $\boldsymbol{A}$ by taking the base 10 logarithm, as described above, and multiply the spectrum by -1 in order to make the absorption features "positive"

$$\boldsymbol{A}(\lambda) = -\log_{10}(\boldsymbol{R}(\lambda)) \tag{4}$$

we convert to energy space, where ν is frequency, as described above

$$\boldsymbol{A}(\nu) = \frac{10\,000}{\boldsymbol{A}(\lambda).} \tag{5}$$

If we consider the absorption bands to be Gaussian in shape, we may model $\boldsymbol{A}(\nu)$ using a series of absorption bands of the following general formula:

$$G(\nu) = \alpha \cdot e^{-\frac{(\nu-\nu_0)^2}{2\sigma^2}} \tag{6}$$

where α is the amplitude (height) of the Gaussian, ν_0 is the central frequency, and σ is the full-width at half-maximum.

If we wish to model the absorption bands as Lorentzian in shape, we may use the formula

$$L(\nu) = \alpha \cdot \left[\frac{\sigma}{(\nu-\nu_0)^2 + \sigma^2}\right]. \tag{7}$$

A Lorentzian shape is often applicable for the absorption bands of gases [18], bought about by collision broadening of line spectra. A Gaussian shape is often superimposed by the effects of instrumental smearing (due to channel bandpass functions), and also by Doppler broadening [22]. Thus, it is often desirable to model the absorption bands as a multiplicative or additive combination of Gaussian or Lorentzian shapes—this is then a Voight profile. An alternative approach, similar to a Voight profile, was suggested by [23] and is adopted here.

If we model the absorption bands using a function K, of the type

$$K(\nu) = \alpha \cdot \left[\frac{1}{(1+\beta^2\psi^2(\nu))^{\frac{1}{\beta^2}}}\right] \tag{8}$$

where

$$\psi(\nu) = \frac{(\nu-\nu_0)}{\sqrt{2}\sigma}. \tag{9}$$

The parameter β is then a reflection of how "Gaussian-like" or "Lorentzian-like" our function is. Here it is called the Voight-likeness parameter. Clearly, if $\beta = 1$, then $K = L$ and we have a Lorentzian shape. If $\beta = 0$, then our expression for K resembles a Gaussian shape.

This is shown if we use the Taylor's theorem expansion for $\ln(1+x)$

$$\ln(1+x) = x - \frac{x^2}{2} + \frac{x^3}{3} - \frac{x^4}{4} + \cdots. \tag{10}$$

Dividing (8) by α, taking the natural logarithm and expanding, we get

$$\begin{aligned}\ln\left(\frac{K}{\alpha}\right) &= -\beta^{-2}\ln(1+\beta^2\psi^2) \\ &= -\psi^2 + \frac{1}{2}\beta^2\psi^4 - \frac{1}{3}\beta^4\psi^6 + \frac{1}{4}\beta^6\psi^8 - \cdots.\end{aligned} \tag{11}$$

Now, we let $\beta = 0$ and take the exponential of both sides to get

$$K = \alpha \cdot e^{-\psi^2}. \tag{12}$$

And hence, $K = G$.

Using our approximation of an absorption band, $K(\nu_0, \alpha, \sigma, \beta)$, we may now approach the problem of fitting our curves to the absorption spectra A in the following way.

Hyperspectral datasets usually do not have enough measured points to carry out least squares analysis. The number of measured points must exceed the number of free parameters [13]. For example, with four free parameters per absorption band, only five bands can be modeled with 21 measured points. Thus, it becomes necessary to interpolate to achieve a greater number of measurement points. This procedure uses an interpolation procedure similar to that described by Dyn *et al.* to model computer graphics curves. This interpolation approximates a cubic spline fit [24]. This interpolation procedure decreases the signal-to-noise ratio (SNR) of the spectrum, so the number of

interpolated points should be kept to a minimum. It was found that two interpolation runs sufficient to achieve good least squares fit, but this is clearly application dependent. Laboratory spectra could be analyzed with no interpolation, for example.

For each absorption band, we must find four parameters, ν_0, α, σ, and β. The central frequency of each peak, ν_0, is found by using an adaptive width sliding window Savitzky–Golay routine to model a sixth-degree polynomial, and calculate the fifth, fourth and second derivatives of this polynomial [25]. A peak is located where the following conditions are fulfilled [12]:

$$\mathrm{A^V}(\nu) = 0, \mathrm{A^{IV}}(\nu) > 0 \text{ and } \mathrm{A^{II}}(\nu) < 0.$$

The superscript in Roman numerals indicates the order of the derivative of the absorption spectra.

The width of the sliding window is crucial to the accuracy of this peak finding method. If the bands are wide, the sliding window should be large to accurately fit the Savitzky–Golay polynomials. The opposite is the case for narrow bands. Huguenin's method of choosing this width is proprietary. This algorithm uses the width of second derivative positive and negative going peaks to approximate the width for each point in the spectrum.

Once the M central peaks are located, we can approximate an initial solution to the other three parameters (α, σ, and β) for each band, K.

To estimate α, we use linear interpolation to estimate the value of $A\ (v)$ at ν_0 for each of the M peaks

$$\alpha_{\mathrm{m}} = A(\nu_{0\mathrm{m}}) \quad \text{where m} = 1, 2, \ldots, \mathrm{M}.$$

To estimate the full-width at half-maximum, σ, we look either side of the peak value, for the closest point in the absorption spectrum $A(v)$ where the value has fallen to half of the value α. The distance either side is calculated, and the smallest distance is taken as the approximation to σ.

The value of β for each absorption band is initially set to a value of 0.5, to approximate an equally mixed Lorentzian-Gaussian curve [26].

Once these initial estimates of the parameters are obtained, we use a two stage iterative least squares method to refine them.

The iterative least squares method minimizes the following relationship:

$$\mathrm{Min}||A - K_{\mathrm{total}}||$$

where $K_{\mathrm{total}} = K_1 + K_2 + \cdots K_{\mathrm{M}}$.

There are many such methods available [13], [27]–[29]—this procedure adopts the well-accepted standard Levenberg–Marquardt (L–M) scheme [13]. The L–M scheme is a cross between Gauss–Newton and steepest descent iterative methods. For each iteration of the L–M scheme, if the chosen parameter set leads to a relatively good improved solution, the next set of parameters are chosen in a method similar to Gauss–Newton. If the solution results are not sufficiently improved, the next parameter set is chosen following the steepest descent method. The L–M scheme is more robust than Gauss–Newton, which can fail to find optimal solutions if the initial parameter choices are poor. It is quicker than steepest descent in well-behaved conditions.

TABLE I
PARAMETERS FOR HUGUENIN'S SYNTHETIC GAUSSIAN ABSORPTION BANDS

Band	ν_0 WAVELENGTH POSITION, CM^{-1}	σ HALF WIDTH, CM^{-1}	α STRENGTH, %A
1	9500	2355	30
2	11500	3040	42
3	14500	1990	30
4	16000	2150	34
5	18500	2033	60
6	20500	2150	80

After the initial estimate and first least squares refinement, the residual error, χ^2 (chi-squared) is calculated

$$\chi^2 = \sqrt{\frac{1}{N}\sum_{n=1}^{N}[A(\nu_n) - K_{\mathrm{total}}(\nu_n)]^2}. \tag{13}$$

If the residual is below a certain threshold, iteration is ended. Threshold values for χ^2 are largely dependent on the dataset being examined, and experimentation with this value is recommended. Values of 0.01 have been quoted in the spectroscopy literature [26] and were found to give acceptable results; however, it was found that values of 1×10^{-3} gave optimal results for the HyMap dataset, which is discussed below. If the χ^2 value does not dip below the threshold after 30 iterations, the loop is exited.

In the first stage of iterative refinement, the ν_0 and β values are pinned at their initial values, and α and σ are allowed to iterate to a close solution. During the second stage, all parameters are free to vary.

This procedure utilizes the best of two techniques that are commonly used separately: the high-order derivative techniques and a staged iterative least squares curve fitting technique. The two-stage enhancement affords stability, since the initial guesses for α and σ for overlapping bands are often variable in accuracy. It also enhances the speed of the curve fitting overall since the starting estimates for the second stage usually require little adjustment.

The curve fitting algorithm was developed using IDL 6.0 from RSI (http://www.rsi.com).

III. SYNTHETIC SPECTRA MODELLING

A continuum removed reflectance spectrum was generated synthetically, and then analyzed to see if the parameters could be retrieved using this curve fitting algorithm.

The parameters for the synthetic spectrum were chosen to be the same as those used by Huguenin to produce his results [12]. The curve parameters appear in Table I. Since Huguenin's spectra were already absorption spectra in energy space, conversion from reflectance was not required. These values were chosen as three pairs of overlapping Gaussian shaped bands, very close to the limit of resolution from each other. Huguenin calculated the limit of resolution of two overlapping curves to be

$$\nu_2 - \nu_1 > 0.56W \tag{14}$$

TABLE II
COMPARISON OF RESULTS FOR CURVE FITTING ALGORITHMS

N	Sampling Resolution in cm^{-1}	Σ_{ERROR} Huguenin's Fifth Derivative Method	Σ_{ERROR} This Paper, Initial β=0.1	Σ_{ERROR} This Paper, Initial β=0.5
88	170.5	148	61	39
100	150	153	48	40
500	30	156	53	24
1000	15	155	79	41

Σ_{error} is the sum (over 6 absorption bands) of the absolute errors in calculated values for v_0.

where W is the widest band's full-width at half-maximum, v_2 and v_1 are their respective central frequencies.

The sum of errors, Σ_{error}, was calculated by summing the absolute difference between the final result for v_0 of each absorption band, and the known, synthetic v_0

$$\Sigma_{\text{error}} = \sum_{m=1}^{M} ||\nu_0(\text{calculated}) - \nu_0(\text{synthetic})||. \quad (15)$$

Huguenin did not specify how many measurement points he used, therefore it was necessary to use a range of values for N. Since parts of Huguenin's technique are proprietary, it cannot be determined how closely his process has been approximated. He quoted a value for Σ_{error} of 143 [12, Table III] for this scenario, which compares favorably to the results that were achieved following his instructions [12].

The algorithm was tested with a range of initial value for β to test the sensitivity of this method to variations in the initial estimate of the β parameter. The results for $\beta = 0.5$, and $\beta = 0.1$ are representative of what was found and are shown here. Sampling resolutions were calculated assuming a measurement range of 15 000 cm^{-1} (from 5000–20 000 cm^{-1}). The results are shown in Table II.

The Σ_{error} figures for different numbers of measurement points illustrate several points.

- The addition of a least squares refinement stage has the capacity to significantly improve (up to three times in this scenario) upon the pure derivative technique.
- Although the synthetic curves were Gaussian, better peak position fits are achievable using an initial Voight-likeness parameter half way between Gaussian and Lorentzian behavior, compared to fits where the Voight likeness parameter was started off closer to a Gaussian shape. This preference for starting values of $\beta = 0.5$ was not reflected in final values of the β parameter—all of which settled below 0.5 and all (bar two) below 0.01 after iterative refinement.
- Little is gained by an order of magnitude increase in N from 100 to 1000, but a value of $N = 88$ is required to reach this stable plateau, since below this value, an extra peak is found in this scenario of six closely spaced bands. For some values of N below 88, the correct number of bands is sometimes found, but in the wrong positions—generally giving Σ_{error} values around 700–1000.

TABLE III
COMPARISON OF RESULTS FOR CURVE FITTING USING INTERPOLATION

N	Points After Interp	Sampling Resoltn in cm^{-1}	Σ_{ERROR} Huguenin's Fifth Derivative Method	Σ_{ERROR} This Paper, Initial β=0.1	Σ_{ERROR} This Paper, Initial β=0.5
		1 interpolation step			
50	99	300	146	86	43
		2 interpolation step			
33	129	454.5	153	103	56
		3 interpolation step			
33	257	454.5	151	105	65
		4 interpolation step			
33	513	454.5	151	61	69
		5 interpolation step			
33	1025	454.5	150	49	150

Σ_{error} is the sum (over 6 absorption bands) of the absolute errors in calculated values for v_0. N is the original number of measurement points before interpolation.

A. Interpolation Sensitivity Testing

In order to test the effectiveness of these interpolation routines, Huguenin's scenario was used with two interpolation runs, and the Σ_{error} was compared. These results appear in Table III.

For values of N less than those shown in Table III, extra peaks were "found" by this curve fitting method. Although good fits were still achieved, an extra peak means the runs cannot be compared by using values for Σ_{error}. Finding an "extra" peak is considered a failure in this analysis, although it should be noted that the results may still give useful information as long as the "found" peaks were small and did not overlap much with real peaks.

The results of running the interpolation routines justifies their use—values for N as low as 33 still gave excellent reproductions of peak positions in this challenging scenario of six overlapping bands.

The trend for better results from mid range values for β is reversed as more interpolation is used. One explanation for this could be that the increasing interpolation is introducing further tendencies toward a Gaussian shape into the data.

It was found that increasing the number of interpolations past 2 did not give any better performance in peak finding for this scenario. The number of final points after interpolation (129 points) is similar to, but slightly larger than, the number of points required for good reproduction of peak positions without interpolation (88 points). This is intuitively reasonable, though an analytical relationship between these two factors has not yet been established.

Since more interpolated points increases computation time without appearing to improve performance (although this has not been exhaustively tested under other scenarios), a standard of two interpolation runs is used for the remainder of this paper.

B. Noise Sensitivity Testing

To test the noise sensitivity of this method another synthetic spectrum simulating the SWIR (4000–5000 cm^{-1}) spectrum of chlorite obtained by a hyperspectral instrument was generated. The parameters of the four bands are given in Table IV. Note

TABLE IV
ABSORPTION BAND PARAMETERS FOR SYNTHETIC CHLORITE SPECTRUM

Band	v_0 WAVELENGTH POSITION, CM^{-1}	σ HALF WIDTH, CM^{-1}	α STRENGTH, %A	β, VOIGHT LIKENESS
1	4500	25	1	0.1
2	4410	60	1.5	0.1
3	4315	50	2	0.1
4	4190	50	2.5	0.1

TABLE V
SYNTHETIC SPECTRAL MODELLING RESULTS FOR VARYING NOISE AND MEASUREMENT POINTS

N	RMS NOISE (IN REFLECTANCE SPACE) 2×10^{-5}	10^{-5}	10^{-6}
20	9	11	3
45	-	3	1
89	-	-	4

Values given are for Σerror, calculated as described in the text. Two interpolation runs were carried out for each scenario. Note that since the peaks were of smaller frequency, the error values are not directly comparable with Tables II and III. A dash means that extra peaks were found so we cannot asses the error. N is the original number of measurement points before interpolation.

they reflect very low absorption depths $(\sim 2\%)$ typical in hyperspectral datasets.

The synthetic spectra were then modeled by the curve fitting algorithm with varying amounts of noise, and varying numbers of measurement points. RMS noise was calculated in reflectance space. Two interpolation runs were used for each scenario. The Σ_{error} was calculated by summing the difference between the calculated and synthetic central wavelengths, v_0. The results appear at Table V. Because the central frequencies are smaller here than for the first example, the results are not directly comparable with Tables II and III.

The noise characteristics of this curve fitting algorithm may be understood in the following way. As explained earlier, the appearance of an extra band is regarded as a failure. When more measurement points are added, more noise is added to each point and more peaks are "found" by the algorithm.

Flat response regions of a spectrum with added noise take on the appearance of small peaks. Since hyperspectral data often show peaks with just one measured point, Fourier smoothing denoising techniques [12] cannot be applied without the risk of eliminating small absorption bands.

The appearance of spurious peaks does not frustrate spectral analysis—these can often be eliminated by careful amplitude thresholding, except where they appear in overlap with other bands. This analysis highlights the critical nature of the noise characteristics of hyperspectral sensors.

C. Gaussian, Lorentz, and Voight Comparison

In order to test the difference between Gaussian, Lorentzian, and Voight curve fitting, a real chlorite SWIR spectrum (obtained from a HyMap dataset) was tested with each type of curve. No noise was added, and two interpolation runs were carried out on an initial number of measurements $N = 23$. Table VI shows the χ^2 values for each type of curve after using this modeling technique.

TABLE VI
COMPARISON OF GAUSSIAN, LORENTZIAN AND VOIGHT FITS

Chi-squared Error	CURVE TYPE GAUSSIAN	LORENTZIAN	VOIGHT
χ^2	0.018	0.026	0.009

Chi squared values calculated for a real chlorite spectrum, fitted using exclusively Gaussian, Lorentzian or Voight type curves.

These results shown in Table VI were typical of SWIR spectra from the HyMap dataset, which is discussed below. The Lorentzian-only curve fits performed the poorest, and the more flexible Voight curves provided the best overall fit. The Lorentzian shapes were probably negatively affected by the fact that continuum removed spectra are being analyzed—the slow fade out to the edges of Lorentzian shapes does not match the sharp edges of continuum removed spectra.

IV. APPLICATION TO HYMAP DATASET

The curve fitting algorithm has been tested on a small subset of a HyMap dataset [5]. The dataset was collected in fine conditions in October 2002 over the Pilbara region of Western Australia [30]. The region is an Archean granite-greenstone terrain, displaying greenschist facies indicator minerals such as chlorite, hornblende, albite, and actinolite. Hydrothermal activity has emplaced muscovite-bearing veins and horizons throughout the terrain. The small scene examined is believed to represent a volcanic edifice, rich in muscovite of varying tetrahedral Al–Si ratio, and surrounded by a chlorite-hornblende rich greenstone region [31]. Pixel resolution is approximately 5 m on the ground. Larger scenes will be investigated in future work.

The investigation was restricted to the SWIR region for the following reasons. The SWIR region is largely unobscured by atmospheric effects. Band saturation is uncommon in the SWIR region due to generally high reflectance [32]. The absorption bands in the SWIR region provide diagnostic information about the presence of hydrous phyllosilicates (such as micas, chlorites, serpentine, talc, etc.) which can be used to map hydrothermally altered zones [33]. Finally, curve fitting the SWIR is attractive due to relatively high SNR achievable in this region with modern instruments (for example, HyMap SNR varies from 250 to 1000 in the SWIR [5]).

Since the HyMap dataset was measured as radiance at sensor, we carried out radiometric correction using the ATREM procedure [34]. This gives an approximation to reflectance on the ground by removing atmospheric-related absorption bands. Following atmospheric correction, the background continuum was removed using automatic continuum removal procedures [21] in order to leave only residual absorption band shapes suitable for modeling. For this study, straight line approximations were made for continuum removal.

Since only the SWIR region of the HyMap dataset has been used, there are $N = 23$ available channels, or measurement points, from 2.0932 to 2.4768 μm. Two interpolation steps were carried out.

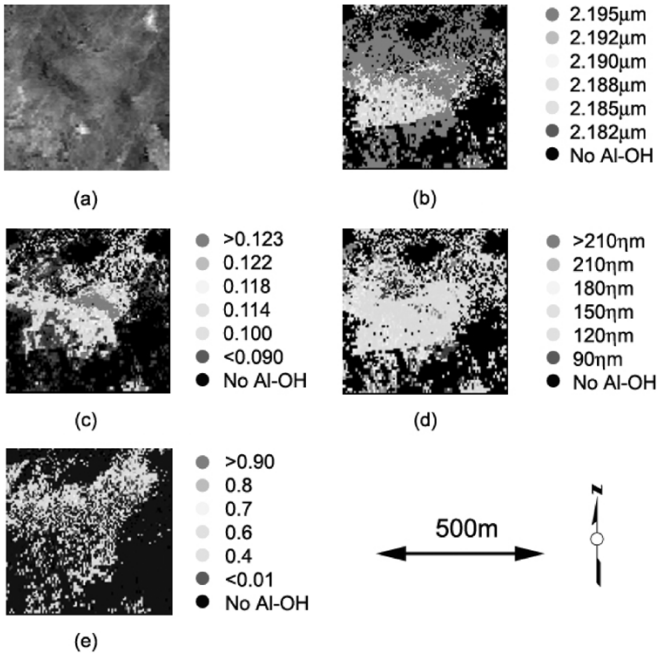

Fig. 2. Maps of Al-OH band parameters. (a) Visible image. (b) Central wavelength, ν_0. (c) Depth of absorption band, α. (d) Full-width at half-maximum, σ. (e) Voight-likeness parameter, β. Values given are the bottom of each range defined by different colors. A supplementary color version is available for download at http://ieeexplore.ieee.org. The file size is 321 KB.

Using the curve fitting algorithm, maps were generated of the Al-OH combination (bend $\delta + \text{stretch}\ \nu$) absorption band near 2.19 μm. This absorption band is indicative of the presence of white mica, such as muscovite. A similar band is also attributable to kaolinite, but this always occurs with another band at 2.16 μm, and in order to find just white mica, all spectra displaying 2.16- and 2.19-μm bands were eliminated.

The results of mapping the 2.19 μm absorption band are shown in Fig. 2. Maps are generated of all four parameters, ν_0, α, σ, and β. Modeling of other absorption bands will be investigated in future work.

The map of central wavelengths [Fig. 2(b)] clearly shows short wavelength Al-OH in a swathe in the middle of the image. This is attributable to high temperature Tschermak substitution [35] in white mica within the volcanic vent. The map of amplitude [Fig. 2(c)] shows a small band of high-amplitude Al-OH in the middle of the image, but not coincident with the regions of low wavelength. This is broadly attributable to the abundance of mica in these locations [6]. The FWHM map [Fig. 2(d)] shows the large preponderance of FWHM at around 150 ηm, although this is variable on the fringes of the white mica-bearing region. The Voight-likeness parameter shows a range of values, mostly from $\beta = 0.4$–0.8, but some of the deepest absorption regions in the center of the image have values around $\beta = 0.9$. This suggests that Voight curves may have more success modeling deeper, narrower absorption bands.

V. Discussion

A. Voight, Lorentzian, or Gaussian?

Research so far has not demonstrated conclusively which type of curve is most suitable for modeling absorption bands in the SWIR region. This method shows Voight-type curves are more flexible and give a better χ^2 fit. The physical significance of the Voight-likeness parameter β has not yet been fully evaluated, but the ability to explore this parameter in future research makes this a valuable addition to the curve fitting algorithm.

B. Asymmetry as a Curve Parameter

In addition to the parameters α, ν_0, σ, and β, the asymmetry of an absorption band can be modeled; however asymmetry can also be caused by hidden overlapping bands. In this study all absorption bands in the SWIR region are assumed to be symmetric and asymmetry is modeled by the fitting of extra absorption bands in the wings of major absorption bands.

C. Continuum Removal or Continuum Modeling?

In order to keep a cap on the free parameters, continuum-removed spectra were used, rather than modeling the continuum. This tends to favor a Gaussian shape rather than Lorentzian shapes (since Gaussian curves fall off more sharply; see Fig. 1). Future work will examine the benefits of continuum modeling.

D. Potential Overfitting of Data

The essence of using an iterative fitting algorithm to model reflectance spectra is the choice of the degrees of freedom employed in the fit. A unique solution to the least squares fitting is not possible [36]. A larger number of absorption bands, and parameters (and hence degrees of freedom), will result in a better fit. Whether the addition of extra absorption bands is justified physically is always open to question. The method outlined in this work, employing a fifth derivative peak fitting algorithm to fix the number of peaks, avoids "overfitting" of the data with extra absorption bands where they may not be justified.

E. Tradeoffs for Using Least Squares Minimization

It is clear that this two-stage method can achieve greater accuracy than derivative techniques. This is mostly attributable to the least squares minimization process. This step is time consuming, and pure derivative methods still have a use as a quick approximation to absorption band central wavelengths.

F. Application to Other Areas of the Spectrum

This curve fitting method has been demonstrated in a limited region of the EM spectrum, namely 2.0–2.5 μm. There is nothing inherently limiting the procedure to this region. The method is also applicable to laboratory or ground-based field spectra, making comparison of results with airborne or satellite spectra convenient.

G. Future Directions in Hyperspectral Sensors

The results of this analysis have highlighted the advantages of higher spectral sampling resolution for future hyperspectral sensors. More measurement points would obviate the need for interpolation runs. This analysis method would immediately benefit from a higher number of spectral channels, even if the channel bandpasses were not improved (although this, too, is of course desirable!). This analysis has also demonstrated the benefits of improvements in hyperspectral instrument SNR.

H. Expert System Analysis

This algorithm returns the number of absorption bands, M, and for each band, the width σ, amplitude α, central wavelength ν_0 and Voight-likeness parameter β. This data can be used as input to an expert system for automatic mineral analysis. Such a system has been described in [37].

VI. Conclusion

A technique for automatic curve fitting of hyperspectral reflectance datasets has been provided and an application provided. This algorithm works by combining fifth derivative peak finding with a multiple stage iterative least squares refinement.

The method provides a repeatable, stable modeling method, preserving the complete shape of the spectra. It employs a Voight-type absorption band curve model. It provides the capability to explore maps of band parameters width σ, amplitude α, central wavelength ν_0, and Voight-likeness parameter β—all of which can be used as an input to an automatic mineral recognition expert system.

Acknowledgment

The generous provision of the HyMap dataset by HyVista and CSIRO is gratefully acknowledged. M. Walter and T. Cudahy are thanked for their supervision of this project.

References

[1] J. W. Boardman, "Automated spectral unmixing of AVIRIS data using convex geometry concepts," presented at the JPL AVIRIS Conf., Pasadena, CA, 1993.

[2] A. A. Green, M. Berman, P. Switzer, and M. D. Craig, "A transformation for ordering multispectral data in terms of image quality with implications for noise removal," *IEEE Trans. Geosci. Remote Sens.*, vol. 26, no. 1, pp. 65–74, Jan. 1988.

[3] T. Isaksson, A. H. Aastveit, J. M. Chalmers, and P. R. Griffiths, Eds., "Classification mthods," in *Handbook of Vibrational Spectroscopy*. New York: Wiley, 2002, pp. 2107–2122.

[4] R. O. Green, M. L. Eastwood, C. M. Sarture, T. G. Chrien, M. Aronsson, B. J. Chippendale, J. A. Faust, B. E. Pavri, C. J. Chovit, M. S. Solis, M. R. Olah, and O. Williams, "Imaging spectroscopy and the Airborne Visible Infrared Imaging Spectrometer (AVIRIS)," *Remote Sens. Environ.*, vol. 65, pp. 227–248, 1998.

[5] T. Cocks, R. Jenssen, A. Stewart, I. Wilson, and T. Shields, "The HyMap airborne hyperspectral sensor: The System, calibration and performance," presented at the 1st EARSeL Conf., 1998.

[6] T. Isaksson, A. H. Aastveit, J. M. Chalmers, and P. R. Griffiths, Eds., "Beer's law," in *Handbook of Vibrational Spectroscopy*. New York: Wiley, 2002, pp. 2225–2234.

[7] R. N. Clark and T. L. Roush, "Reflectance spectroscopy: Quantitative analysis techniques for remote sensing applications," *J. Geophys. Res.*, vol. 89, pp. 6329–6340, 1984.

[8] J. M. Hunt and D. S. Turner, "Determination of mineral constituents of rocks by infrared spectroscopy," *Anal. Chem.*, vol. 25, pp. 1169–1174, 1953.

[9] G. R. Hunt, "Spectral signatures of particular minerals in the visible and near infrared," *Geophysics*, vol. 42, pp. 501–513, 1977.

[10] W. L. Butler, "Fourth derivative spectra," *Methods Enzymol.*, vol. 56, pp. 501–515, 1979.

[11] T. H. Demetriades-Shah, M. D. Steven, and J. A. Clark, "High resolution derivative spectra in remote sensing," *Remote Sens. Environ.*, vol. 33, pp. 55–64, 1990.

[12] R. L. Huguenin and J. L. Jones, "Intelligent information extraction from reflectance spectra: Absorption band positions," *J. Geophys. Res.*, vol. 91, pp. 9585–9598, 1986.

[13] P. R. Bevington and D. K. Robinson, *Data Reduction and Error Analysis for the Physical Sciences*, 2nd ed. New York: McGraw-Hill, 1992.

[14] R. N. Clark, "Water frost and ice: The near-infrared spectral reflectance 0.65–2.5 microns," *J. Geophys. Res.*, vol. 86, pp. 3087–3096, 1981.

[15] J. M. Sunshine, C. M. Pieters, and S. F. Pratt, "Deconvolution of mineral absorption bands: An improved approach," *J. Geophys. Res.*, vol. 95, pp. 6955–6966, 1990.

[16] K. H. Michaelian, W. I. Friesen, S. Yariv, and A. Nasser, "Diffuse reflectance infrared spectra of kaolinite and kaolinite/alkali halide mixtures. Curve fitting of the OH stretching region," *Can. J. Chem.*, vol. 69, pp. 1786–1790, 1991.

[17] R. N. Jones, "Computer programs for Infrared spectrophotometry," *Bull.—Nat. Res. Council Canada*, vol. 11–17, 1977.

[18] K. S. Seshadri and R. N. Jones, "The shapes and intensities of infrared absorption bands—A review," *Spectrochimica Acta*, vol. 19, pp. 1013–1085, 1963.

[19] M. Paterson, "The determination of hydroxyl by infrared absorption in quartz, silicate glasses and similar materials," *Bull. Mineralogie*, vol. 105, pp. 20–29, 1982.

[20] G. R. Rossman, "Vibrational spectroscopy of hydrous components," in *Spectroscopic Methods in Mineralogy and Geology: Mineralogical Society of America Reviews in Mineralogy*, F. C. Hawthorne, Ed., 1988, vol. 18, pp. 193–206.

[21] R. N. Clark, T. V. V. King, and N. Gorelick, "Automatic continuum analysis of reflectance spectra," presented at the Proceedings of the 3rd Airborne Imaging Spectrometer Data Analysis Workshop, Pasadena, CA, 1987.

[22] J. J. Turner, A. H. Aastveit, J. M. Chalmers, and P. R. Griffiths, Eds., "Bandwidths," in *Handbook of Vibrational Spectroscopy*. New York: Wiley, 2002, pp. 101–127.

[23] R. D. B. Fraser and E. Suzuki, "Resolution of overlapping bands: Functions for simulating band shapes," *Anal. Chem.*, vol. 41, pp. 37–39, 1969.

[24] N. Dyn, J. Gregory, and D. Levin, "A 4-point interpolatory subdivision scheme for curve design," *Comput. Aided Geom. Des.*, vol. 4, pp. 257–268, 1987.

[25] A. Savitzky and M. J. E. Golay, "Smoothing and differentiation of data by simplified least squares procedures," *Anal. Chem.*, vol. 36, pp. 1627–1639, 1964.

[26] F. Alsmeyer and W. Marquardt, "Automatic generation of peak-shaped models," *Appl. Spectrosc.*, vol. 58, pp. 986–994, 2004.

[27] A. Tarantola and B. Valette, "Generalized nonlinear inverse problems solved using the least squares criterion," *Rev. Geophys.*, vol. 20, pp. 219–232, 1982.

[28] H. G. Kaper, D. W. Smits, U. Schwarz, K. Takakubo, and H. Van Woerden, "Computer analysis of observed distributions into gaussian components," *Bull. Astron. Inst. Netherlands*, vol. 18, pp. 465–487, 1966.

[29] W. H. Press, B. P. Flannery, S. A. Teukolsky, and W. T. Vetterling, *Numerical Recipes in Pascal*. New York: Cambridge Univ. Press, 1989.

[30] A. J. Brown, M. R. Walter, and T. J. Cudahy, "Hyperspectral imaging spectroscopy of a mars analog environment at the North Pole dome," *Pilbara Craton, Western Australia, Australian J. Earth Sci.*, vol. 52, pp. 353–364, 2005.

[31] M. J. Van Kranendonk, *Geology of the North Shaw 1:100 000 Sheet*, 1st ed. Perth, Australia: Geol. Surv. Western Australia, Dept. Minerals and Energy, 2000.

[32] R. V. Morris, S. C. Neely, and W. W. Mendell, "Application of Kubelka-Munk theory of diffuse reflectance to geologic problems: The role of scattering," *Geophys. Res. Lett.*, vol. 9, pp. 113–116, 1982.

[33] G. R. Hunt, "Near infrared (1.3–2.4 μm) spectra of alteration minerals-potential for use in remote sensing," *Geophysics*, vol. 44, pp. 1974–1986, 1979.

[34] B.-C. Gao, K. B. Heidebrecht, and A. F. H. Goetz, "Derivation of scaled surface reflectances from AVIRIS data," *Remote Sens. Environ.*, vol. 44, pp. 165–178, 1993.

[35] E. F. Duke, "Near infrared spectra of muscovite, Tschermak substitution, and metamorphic reaction progress: Implications for remote sensing," *Geology*, vol. 22, pp. 621–624, 1994.

[36] B. G. M. Vandeginste and L. De Galan, "Critical evaluation of curve fitting in infrared spectrometry," *Anal. Chem.*, vol. 47, pp. 2124–2132, 1975.

[37] R. N. Clark, G. A. Swayze, K. E. Livo, R. F. Kokaly, S. J. Sutley, J. B. Dalton, R. R. McDougal, and C. A. Gent, "Imaging spectroscopy: Earth and planetary remote sensing with the USGS tetracorder and expert systems," *J. Geophys. Res.*, vol. 108, pp. 5131–5175, 2003.

Adrian Jon Brown received the B.E. (Hons.) degree from the University College, University of New South Wales, Australian Defence Force Academy, Sydney, in 1994 and the Master's degree in computer studies from the University of New England, Portland, ME, in 2000.

He spent 11 years in the Royal Australian Navy as a Weapons Engineer, followed by a period of contract work as a software engineer for IBM. He is currently based at Macquarie University, Sydney.